Flow past a circular cylinder on a β-plane

E. R. Johnson and M. A. Page

Link to this article: http://journals.cambridge.org/abstract_S0022112093003544

How to cite this article:
E. R. Johnson and M. A. Page (1993). Flow past a circular cylinder on a β-plane. Journal of Fluid Mechanics, 251, pp 603-626 doi:10.1017/S0022112093003544

Request Permissions : Click here

Flow past a circular cylinder on a β-plane

By E. R. JOHNSON[1] AND M. A. PAGE[2]

[1] Department of Mathematics, University College London, Gower Street,
London WC1E 6BT, UK

[2] Department of Mathematics, Monash University, Clayton, Victoria 3168, Australia

This paper gives analytical and numerical solutions for both westward and eastward flows past obstacles on a β-plane. The flows are considered in the quasi-geostrophic limit where nonlinearity and viscosity allow deviations from purely geostrophic flow. Asymptotic solutions for the layer structure in almost-inviscid flow are given for westward flow past both circular and more elongated cylindrical obstacles. Structures are given for all strengths of nonlinearity from purely linear flow through to strongly nonlinear flows where viscosity is negligible and potential vorticity conserved. These structures are supported by accurate numerical computations. Results on detraining nonlinear western boundary layers and corner regions in Page & Johnson (1991) are used to present the full structure for eastward flow past an obstacle with a bluff rear face, completing previous analysis in Page & Johnson (1990) of eastward flow past obstacles without rear stagnation points. Viscous separation is discussed and analytical structures proposed for separated flows. These lead to predictions for the size of separated regions that reproduce the behaviour observed in experiments and numerical computations on β-plane flows.

1. Introduction

Perhaps the simplest motion for a homogeneous, constant-depth ocean on the rotating Earth is that of uniform flow along parallels of latitude. When these parallels are interrupted by ocean boundaries or isolated islands, thin layers form where unsteadiness, nonlinear advection or viscosity become equally as important as Coriolis and pressure gradient forces. One of the most straightforward problems where these effects can be investigated is flow past obstacles on a β-plane. Foster (1985) discusses uniform eastward flow past a cylinder, showing that the linear solution depends on a parameter α measuring the ratio of the β-effect to Ekman pumping destruction of vorticity, and that nonlinear effects are given by a parameter λ measuring the ratio of advection to Ekman pumping terms. Foster presents the asymptotic form of the almost-inviscid solution when $\alpha \gg 1$ and discusses the first effects of nonlinearity which appear as λ increases to be of order $\alpha^{-1} \ll 1$. Foster notes difficulties with the flow at the rear stagnation point and in obtaining solutions for westward flows. Matsuura & Yamagata (1986) present numerical computations for equations modelling viscous flow on a β-plane. They note that although there is a well-defined 'Long's model' solution (Long 1952) for westward flow, the predicted flow patterns differ greatly from experimental observations by Long himself and Boyer & Davies (1982). Matsuura & Yamagata's integrations reproduce many of the aspects of the observed flows and they ascribe the difference from Long's solutions to westward propagating waves.

The problem of eastward flow is also considered in Page & Johnson (1990, hereafter

referred to as I) where the forms of the flow for various α and λ are discussed supported by numerical integrations of the equation of motion for arbitrary α, λ. This work emphasizes the upstream (westward) influence of obstacles and confirms the difficulties of obtaining a simple structure at the rear stagnation point. In fact numerical solutions are presented for an aerofoil-shaped obstacle so the rear stagnation point is absent and vorticity-carrying fluid is shed smoothly from the rear of the obstacle. A structure for the rear stagnation point can however be obtained following the analysis in Page & Johnson (1991, hereafter referred to as II) which considers the more general problem of detraining stagnation-point flow in a western boundary current, formed for example by the collision of northward and southward western boundary jets.

It is the purpose of the present paper to extend the results and methods of I and II to present asymptotic structures for

(i) almost-inviscid westward flow for all values of flow speed from $\lambda = 0$ through $\lambda \sim \alpha^{-1}$ to $\lambda \sim 1$ and $\lambda \sim \alpha \gg 1$,

(ii) eastward flow past bodies with bluff rear profiles when $\lambda \sim \alpha^{-1}$,

(iii) separated viscous westward flows,

and to discuss these in the context of previous observations and numerical computations.

Section 2 describes the almost-inviscid limit, giving the governing equations and noting the method used to integrate the equations numerically to obtain solutions for comparison with the postulated asymptotic forms. Section 3 deals with westward flow. Section 3.1 summarizes briefly results for linear ($\lambda = 0$) flow past a cylinder for later reference. Section 3.2 presents, for arbitrary α and λ, a solution for an entraining stagnation point in a western boundary layer (WBL), which gives *inter alia* the localized structure at the front stagnation point of the cylinder. Section 3.2 also gives a solution for a detraining stagnation point of in an eastern boundary jet, depending on advection for its existence, and giving the localized structure for the rear stagnation-point flow on the cylinder that appears once λ exceeds $\frac{1}{4}\alpha^{-1}$. Section 3.3 gives the form of the flow when λ is of order α^{-1}, i.e. $\bar{\lambda} = \alpha\lambda$ is of order unity, and nonlinearity first becomes important in the WBL. It is shown in §3.3.1 that provided $\bar{\lambda} \leqslant \frac{1}{4}$ flow outside the WBL is unaltered from linear flow, with fluid from the layer passing through regions at the shoulders (widest points) of an obstacle to enter shear layers that spread downstream to the west. Section 3.3.2 shows however that once $\bar{\lambda}$ exceeds $\frac{1}{4}$ some fluid from the WBL continues round an obstacle to form a detraining eastern boundary jet and less fluid enters the shear layers directly. Section 3.4 shows that once λ is of order unity ($\bar{\lambda} \gg 1$) the flow has completely changed from linear flow. The WBL is thicker and no longer affected by viscosity, the shear layers originating from the shoulder regions are absent, and all fluid from the WBL continues smoothly round the obstacle to form a detraining eastern boundary jet. Section 3.5 shows that with increasing λ this solution joins smoothly to that obtained in purely inviscid flow from a 'Long's model' type integration, conserving potential vorticity along streamlines from a region of uniform flow far upstream. Section 3.6 discusses modifications to the structure when obstacles have boundaries with regions of finite length lying precisely east–west. Eastward flow is considered in §4.

The solutions of §§3, 4 for almost-inviscid flow require horizontal viscous effects to be confined to thin attached vertical boundary layers against obstacles. Provided these $E^{\frac{1}{4}}$ layers (where E is an Ekman number for the flow) remain attached the solutions can be expected to predict well flows of real fluids of small but non-zero viscosity. Section 5 discusses the behaviour of the $E^{\frac{1}{4}}$ layers on a circular cylinder noting that for moderate and large $\bar{\lambda}$ the layers are likely to separate. Once the $E^{\frac{1}{4}}$ layers separate the

flow pattern can differ significantly from the analytical and numerical solutions in §§3, 4. However the analysis of §3 allows the form of the separated solution to be obtained immediately over a wide range of λ. Section 5 predicts flow patterns consistent with both Matsuura & Yamagata's calculations and Boyer & Davies' experiments, giving a scaling for the size of the separated region that reproduces all the qualitative variation observed in their experiments.

The relationships between the various structures and previous work are summarized in §6.

2. The governing equations

Consider a homogeneous fluid of density ρ^* and kinematic viscosity ν^* of average depth d^* rotating at angular velocity Ω^* about a vertical axis Oz^*, and choose coordinates $Ox^*y^*z^*$ fixed in a frame of reference rotating with the fluid. Let the base of the container be inclined at a small angle β from the horizontal so that it slopes upward in the y^* direction. Let a cylindrical obstacle with vertical generators and width of order l^* occupy the whole fluid depth in the neighbourhood of the origin (see I for example). Suppose that at $t^* = 0$ the fluid at large distance is set into uniform motion along lines of constant depth at speed U^*. It is noted in I that the four non-dimensional parameters

$$Ro = U^*/\Omega^*l^*, \quad E = \nu^*/\Omega^*d^{*2}, \quad \tan\beta, \quad d = d^*/l^*, \tag{2.1}$$

the Rossby number, Ekman number, bottom slope and scaled depth respectively, are sufficient to describe the flow. Further for almost-inviscid flow, where E, Ro, and β are small, motion is two-dimensional with horizontal velocity components given by the geostrophic relations

$$u = -\psi_y, \quad v = \psi_x, \tag{2.2}$$

where $2\rho^* U^*\Omega^* l^*\psi$ is the deviation of the pressure from its equilibrium value. The flow is governed by the equation for the vertical component of relative vorticity, $\zeta = v_x - u_y = \nabla^2\psi$,

$$\tau\zeta_t + \lambda(u\zeta_x + v\zeta_y) + \alpha v + \zeta = 0. \tag{2.3}$$

Here t is time scaled on Ω^*, all lengths have been scaled on l^* and velocities on U^*. The parameter $\tau = \frac{1}{2}E^{-\frac{1}{2}}$ is the scaled Ekman spinup time and

$$\alpha = \frac{\tan\beta}{dE^{\frac{1}{2}}}, \quad \lambda = \frac{Ro}{2E^{\frac{1}{2}}}. \tag{2.4}$$

Equation (2.3) follows from the full Navier–Stokes equations in the formal limit $\tan\beta \to 0$, $Ro \to 0$, $E \to 0$ with α, λ, d fixed. In this limit the Reynolds number $U^*l^*/\nu^* = Ro/d^2E$ is infinite and the flow is effectively inviscid. The sole viscous effect is destruction of vorticity by Ekman pumping represented by the final term on the left-hand side of (2.3). Horizontal viscous effects are absent from the bulk of the fluid and the flow satisfies the usual inviscid impermeability conditions on solid boundaries. Vertical boundary layers within which the horizontal viscous terms are important form against solid boundaries. These layers and their possible separation are discussed in greater detail in §5.

The sloping-bottom configuration is equivalent at leading order to the β-plane approximation in geophysical flows where the depth is constant, and the flow is taken to be rotating at the dimensional rate $\frac{1}{2}(f^* + \beta^*y^*)$. The sole change is the replacement of $\tan\beta$ by β^*d^*/f^* and Ω^* by $\frac{1}{2}f^*$. The Oy-direction is then northward and Ox

eastward. When the obstacle is a circular cylinder the impermeability and far-field conditions become

$$\psi = 0 \quad (x^2 + y^2 = 1, t > 0),$$ (2.5)

$$\nabla\psi \to (0, \pm 1) \quad (x^2 + y^2 \to \infty, t > 0),$$ (2.6)

where the positive sign corresponds to westward flow at large distances and the negative sign to eastward flow.

This paper considers steady solutions of (2.3), in particular asymptotic solutions in the limit of weak Ekman pumping, $\alpha \gg 1$. These structures are supported by numerical integrations of the initial value problem for (2.3) subject to (2.5), (2.6) and the condition that the flow is irrotational initially. The numerical method consists of introducing an outer sidewall at $y \sim W \gg 1$, mapping the resulting variable-width channel to a constant-width channel and treating this simpler domain in Cartesian coordinates. The vorticity equation (2.3) is integrated forward in time using a modified ADI method and at each time-step the resulting Poisson equation for the streamfunction is solved by cyclic reduction. A radiation boundary condition is applied far upstream to allow the most slowly decaying mode to propagate out of the domain, and far downstream the flow is taken to decay exponentially towards uniform flow, with the only modification here being a straightforward change to the radiation boundary conditions to make them appropriate for westward flows. Further details of the method and discussion of the radiation condition and decay rates are given in I.

3. Westward flow

3.1. *Slow flow; α arbitrary, λ small*

For slow steady flow with $\lambda \ll \min(\alpha^{-1}, 1)$ the vorticity equation (2.3) reduces to

$$\nabla^2\psi + \alpha\psi_x = 0,$$ (3.1)

whose exact solution subject to (2.5) and (2.6) for westward flow is

$$\psi = y - 2\exp(-\tfrac{1}{2}\alpha x) \sum_{n=1}^{\infty} nI_n(\tfrac{1}{2}\alpha)[K_n(\tfrac{1}{2}\alpha r)/K_n(\tfrac{1}{2}\alpha)]\sin n\theta,$$ (3.2)

where r and θ are the usual polar coordinates. Solution (3.2) reduces to potential flow in the limit $\alpha \to 0$ when the β-effect is weak. Figure 1 gives streamline patterns for $\alpha = 1$ and 32. As α increases and viscosity becomes less important in the bulk of the fluid a stagnant region appears and grows downstream of the cylinder, the WBL in front of the cylinder thins and the shear layer matching the wake to the undisturbed flow also thins and lengthens. The remainder of this paper concentrates on the weakly viscous limit of $\alpha \gg 1$. Viscous effects are thus weak outside layers thin compared to the cylinder diameter. A full discussion of the asymptotic properties at large α of the series in (3.2) follows from the methods introduced by Waechter (1968) in discussing the motion of a cylinder in a conducting fluid. The series analysed there and described further in Waechter & Phillips (1985) for flow in unsaturated soil is the θ-derivative of (3.2). A related series also appears in the discussion in Hide & Hocking (1979) of flow within a sliced cylinder. For present purposes, the asymptotic results of Foster (1985) are sufficient.

On scales of order the cylinder diameter the flow is purely westward with

$$\psi = \begin{cases} 0, & x < -(1-y^2)^{\frac{1}{2}}, |y| < 1 \\ y, & \text{otherwise.} \end{cases}$$ (3.3)

The flow is unperturbed approaching the cylinder from the east. Incident streamlines are turned within a boundary layer of thickness α^{-1} on the leading half of the cylinder
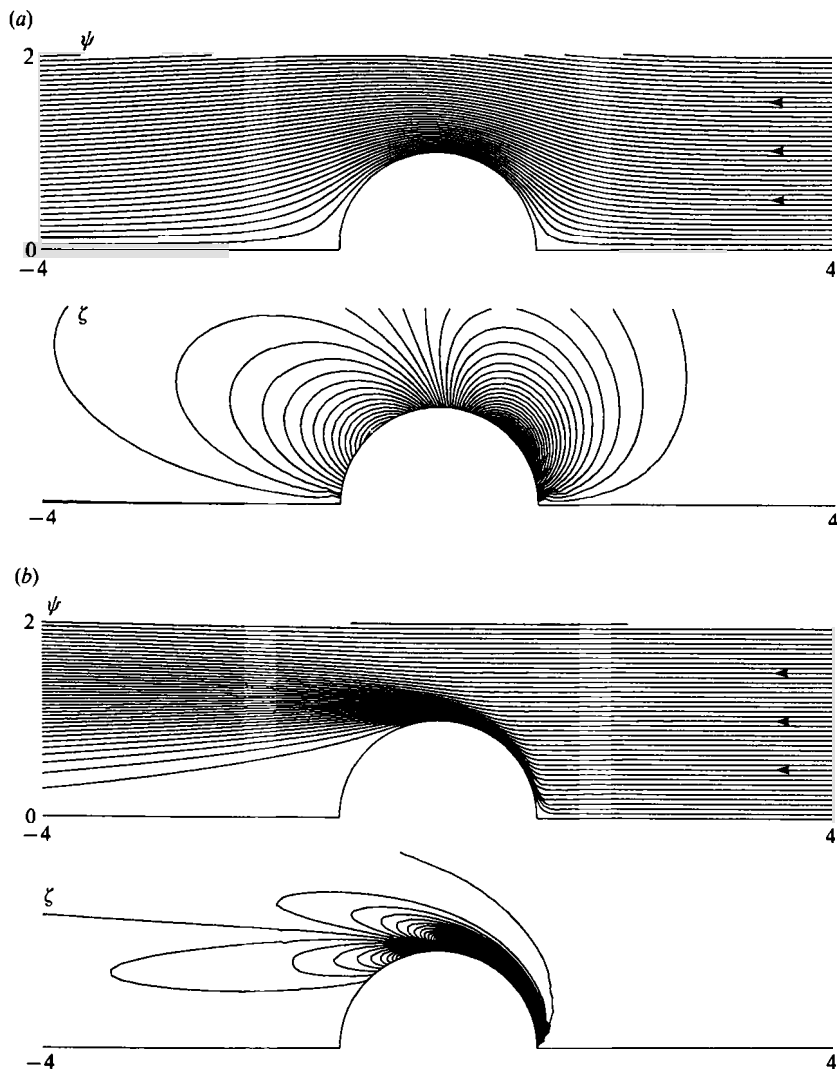
(a)

(b)

FIGURE 1. Streamline and vorticity patterns for linear westward flow past a circular cylinder. (a) $\alpha = 1$, (b) $\alpha = 32$. The streamline interval in this and all streamline patterns except figure 7 is 0.05. The vorticity contour interval is 0.05 in (a) and 2 in (b).

to form northward and southward WBLs each carrying by $(x, y) = (0, \pm 1)$ the unit flux incident on the cylinder between $y = 0$ and $y = \pm 1$. It is here that with increasing flow speed advection first becomes important and these nonlinear effects are discussed in the remainder of this section. The fluid from the WBLs passes through shoulder regions at $(0, \pm 1)$ of dimensions $\alpha^{-\frac{1}{3}} \times \alpha^{-\frac{2}{3}}$, spreading to form a mass source for shear layers stretching along $y = \pm 1$ in $x < 0$. These layers carry unit flux, and for $-x$ of order unity have thickness of order $\alpha^{-\frac{1}{2}}$. The two layers have identical structure. In particular the layer about $y = 1$ is governed by the parabolic equation and leading-order (in α^{-1}) boundary condition

$$\psi_{\hat{y}\hat{y}} + \psi_x = 0 \quad (-x > 0), \tag{3.4}$$

$$\psi(0, \hat{y}) = \begin{cases} 1, & \hat{y} > 0 \\ 0, & \hat{y} < 0, \end{cases} \tag{3.5}$$
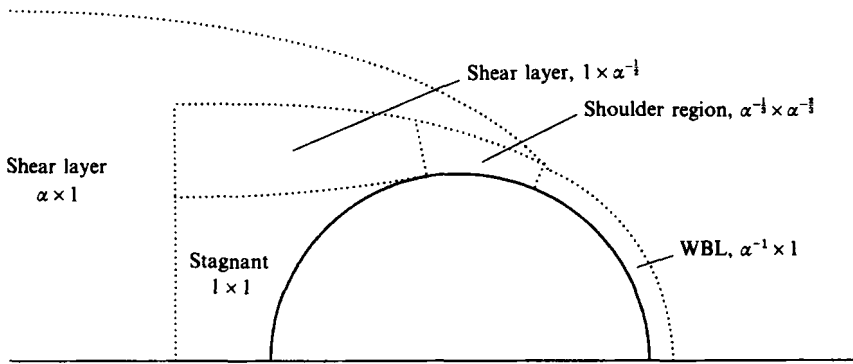
FIGURE 2. A schematic diagram of the various linear ($\lambda = 0$) flow regimes and their sizes in the asymptotic limit of almost inviscid flow, $\alpha \gg 1$. All fluid incident on the cylinder between $y = 0$ and $y = 1$ is turned by the WBL to pass through the shoulder region and be emitted through a source of unit strength into the spreading shear layer, which is of thickness $\alpha^{-\frac{1}{2}}$ for $-x$ of order unity but spreads to have unit width and merge with the equivalent layer about $y = -1$ when $-x$ is of order α.

where $\hat{y} = \alpha^{\frac{1}{2}}(y-1)$ and $-x$ is a time-like variable. The layers spread with increasing $-x$ and merge for $-x$ of order α (figure 2). Foster (1985) notes that the treatment of the source and merging regions can be combined by introducing $X = \alpha^{-1}x$ so that

$$\psi_{yy} + \psi_X = 0 \quad (-X > 0), \tag{3.6}$$

$$\psi(0, y) = \begin{cases} y, & |y| > 1 \\ 0, & |y| < 1. \end{cases} \tag{3.7}$$

It is shown in succeeding sections that with increasing flow speed the equations governing the shear layers remain unaltered but the boundary conditions (3.5), (3.7) change and hence the flow in the layers is altered.

3.2. Stagnation-point flow in the western boundary layer

Close to the forward stagnation point at $(x, y) = (1, 0)$ the cylinder is locally planar and the oncoming flow near the centreline $y = 0$ is uniform. The governing equation (2.3) in this region has a similarity solution of the form

$$\psi = yF(x), \tag{3.8}$$

provided

$$\lambda(F'F' - FF'') + F' + \alpha F = \alpha, \tag{3.9}$$

where $F(0) = 0$ and $F(\infty) = 1$. The system has the exact solution

$$F(x) = 1 - \exp(-x/\delta), \tag{3.10}$$

provided

$$\alpha\delta^2 - \delta - \lambda = 0. \tag{3.11}$$

This gives a boundary layer of thickness $\delta > 0$ with

$$\delta = [1 + (1 + 4\alpha\lambda)^{\frac{1}{2}}]/2\alpha. \tag{3.12}$$

The solution exists for all values of the flow speed λ. In addition to giving the local solution for flow near the forward stagnation point in westward flow past a cylinder, (3.8)–(3.12) give the complete solution for westward flow towards a planar wall at $x = 0$. The uniform westward flow splits, turning to form northward and southward boundary jets which entrain fluid at a constant rate as they move away from the

stagnation point. Their thickness δ remains constant and so the velocity in the jets increases linearly with distance from the stagnation point. For large α and $\lambda \ll \alpha^{-1}$ the layer thickness $\delta \sim \alpha^{-1}$, the layer thickness in linear flow. The layer thickens with increasing flow speed λ although remaining of order α^{-1} for $\lambda \sim \alpha^{-1} \ll 1$. For λ of order unity δ is of order $\alpha^{-\frac{1}{2}}$, much thicker than the linear layer. For almost inviscid flow where $\lambda \sim \alpha \gg 1$ the layer has thickness of order unity and westward flow past a cylinder turns on scales of order the cylinder diameter. The limits can be combined by introducing

$$b = (\lambda/\alpha)^{\frac{1}{2}} = Ro/\beta, \tag{3.13}$$

the Rossby wave scale (the reciprocal of the wavenumber κ in I) determined by β and the flow speed. Once λ is of order α^{-1} or larger the boundary jets have thickness of order b. The three distinguished limits $\lambda \sim \alpha^{-1}$, $\lambda \sim 1$, $\lambda \sim \alpha$ are described in the following subsections.

The second root of (3.11) is negative giving a detraining eastern boundary layer of thickness

$$-\delta = [(1+4\alpha\lambda)^{\frac{1}{2}} - 1]/2\alpha. \tag{3.14}$$

This layer depends on advection for its existence, having thickness of order λ for $\lambda \ll 1$ and thickness of order b once λ is of order α^{-1} or larger. It is shown in §§3.4, 3.5 that this flow appears at the rear stagnation point of the cylinder for $\lambda \gg \alpha^{-1}$.

These stagnation-point solutions relate closely to general boundary-layer solutions. At the outer edges of the boundary layers the flow deviates locally only slightly from uniform flow. Linearizing about this uniform flow gives precisely solution (3.10). The values of δ give the asymptotic form of the outer boundary-layer structure and, in particular, the entraining WBL corresponding to (3.12) can match an arbitrary incoming flow. This point is discussed further for detraining layers in §4.1.

3.3. *The flow field for* $\lambda \sim \alpha^{-1}, \alpha \gg 1$

With increasing flow speed the advection of vorticity first becomes important in the WBL which becomes nonlinear for $\lambda \sim \alpha^{-1}$, as Foster (1985) notes for eastward flow. In the layer the vorticity equation (2.3) becomes

$$\bar{\lambda}(\tilde{u}\tilde{\zeta}_\xi + \tilde{v}\tilde{\zeta}_\theta) + \tilde{\zeta} + \tilde{v}\cos\theta = 0, \tag{3.15}$$

where $\bar{\lambda} = \alpha\lambda$, $\xi = \alpha(r-1)$. The velocity components in the r- and θ-directions are

$$\tilde{u} = -\psi_\theta, \quad \tilde{v} = \psi_\xi, \tag{3.16}$$

and the vorticity has the single component, $\tilde{\zeta} = \tilde{v}_\xi$. Values of $\tilde{v}, \tilde{\zeta}$ of order unity thus correspond to azimuthal velocities of order $\alpha \gg 1$ and vorticuty of order α^2. As noted in §3.2 the asymptotic form for the outer edge of the layer can match an arbitrary entraining outer flow. The layer thus satisfies the zero-normal-flow and far-field conditions

$$\psi(0,\theta) = 0, \quad \psi(\infty,\theta) = \psi_\infty(\theta), \tag{3.17}$$

where $\psi_\infty(\theta)$ is the streamfunction value at the outer edge of the layer. Here

$$\psi_\infty(\theta) = \sin\theta, \quad (0 < \theta < \tfrac{1}{2}\pi). \tag{3.18}$$

Since the flow field for large ξ is known completely, (3.15) can be integrated once directly to yield

$$\bar{\lambda}(\tilde{u}\tilde{v}_\xi + \tilde{v}\tilde{v}_\theta) + \tilde{v} + \psi\cos\theta = \psi_\infty(\theta)\cos\theta. \tag{3.19}$$

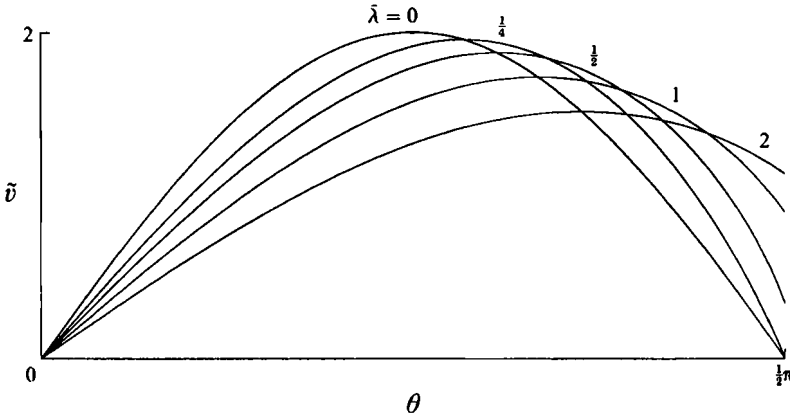Equation (3.19) can be integrated further most straightforwardly by introducing a

FIGURE 3. The scaled tangential velocity $\tilde{v}$ against the surface of the cylinder when $\bar{\lambda} = \alpha\lambda$ is of order unity. The velocity is plotted as a function of θ from the front stagnation point at $\theta = 0$ to the shoulder region at $\theta = \frac{1}{2}\pi$. For $\bar{\lambda} \leqslant \frac{1}{4}$ the velocity vanishes at $\theta = \frac{1}{2}\pi$ and the end of the WBL is like stagnation-point flow. However for $\bar{\lambda} > \frac{1}{4}$, $\tilde{v}$ is non-zero and fluid from the WBL continues as a narrow boundary jet.

Von-Mises transformation from (ξ, θ) to (ψ, θ) as in Foster (1985) and II. Along lines of constant ψ, (3.19) reduces to the ordinary differential equation

$$\bar{\lambda}\tilde{v}\tilde{v}_\theta + \tilde{v} + \psi \cos\theta = \psi_\infty(\theta)\cos\theta, \qquad (3.20)$$

giving $\tilde{v}$ as a function of θ. The far-field condition (3.17) shows that the incident streamline with $\psi = \psi_0$ ($0 \leqslant \psi_0 \leqslant 1$) originates along $\theta = \theta_0 = \sin^{-1}\psi_0$. At large distances the flow is uniform and so $\tilde{v}$ vanishes. Hence the integration of (3.20) along the streamline $\psi = \psi_0$ starts at $\theta = \theta_0$ with initial condition $\tilde{v} = 0$ and proceeds with increasing θ to the end of the layer at $\theta = \frac{1}{2}\pi$. Figure 3 gives, for various values of the oncoming flow strength $\bar{\lambda}$, the velocity $\tilde{v}$ at the surface of the cylinder obtained by integrating (3.19) along $\psi = 0$ away from the forward stagnation point. The azimuthal velocity $\tilde{v}$ vanishes at $\theta = \frac{1}{2}\pi$ provided $\bar{\lambda} \leqslant \frac{1}{4}$ but is non-zero there for $\bar{\lambda} > \frac{1}{4}$. This difference changes the whole local structure of the solution. The two forms are discussed in the following subsections.

3.3.1. *The flow field for* $\bar{\lambda} = \lambda\alpha \leqslant \frac{1}{4}$, $\alpha \gg 1$

As $\bar{\lambda}$ increases from zero the WBL retains the same general form as the linear layer of §3.1. The layer entrains fluid from the incident uniform stream and carries it round the cylinder until the layer ends at $\theta = \frac{1}{2}\pi$. The linear solution on this scale at the layer end is locally like stagnation-point flow as the WBL of thickness α^{-1} expands to join the shoulder region of thickness $\alpha^{-\frac{2}{3}}$ before passing to the shear layer about $y = 1$. The nonlinear layer is not so restricted. Equation (3.20) requires only that on each streamline

$$\tilde{v}(\bar{\lambda}\tilde{v}_\theta + 1) = 0, \quad (\theta = \frac{1}{2}\pi). \qquad (3.21)$$

Hence either $\tilde{v}$ vanishes and the flow is locally stagnation-like or $\tilde{v}_\theta = -1/\bar{\lambda}$. For $\bar{\lambda} \leqslant \frac{1}{4}$ a stagnation solution can be obtained similarly to that for eastward flow in Foster (1985) by seeking a solution of the form

$$\psi = G((\tfrac{1}{2}\pi - \theta)\,\xi). \qquad (3.22)$$

Substituting in (3.15) gives

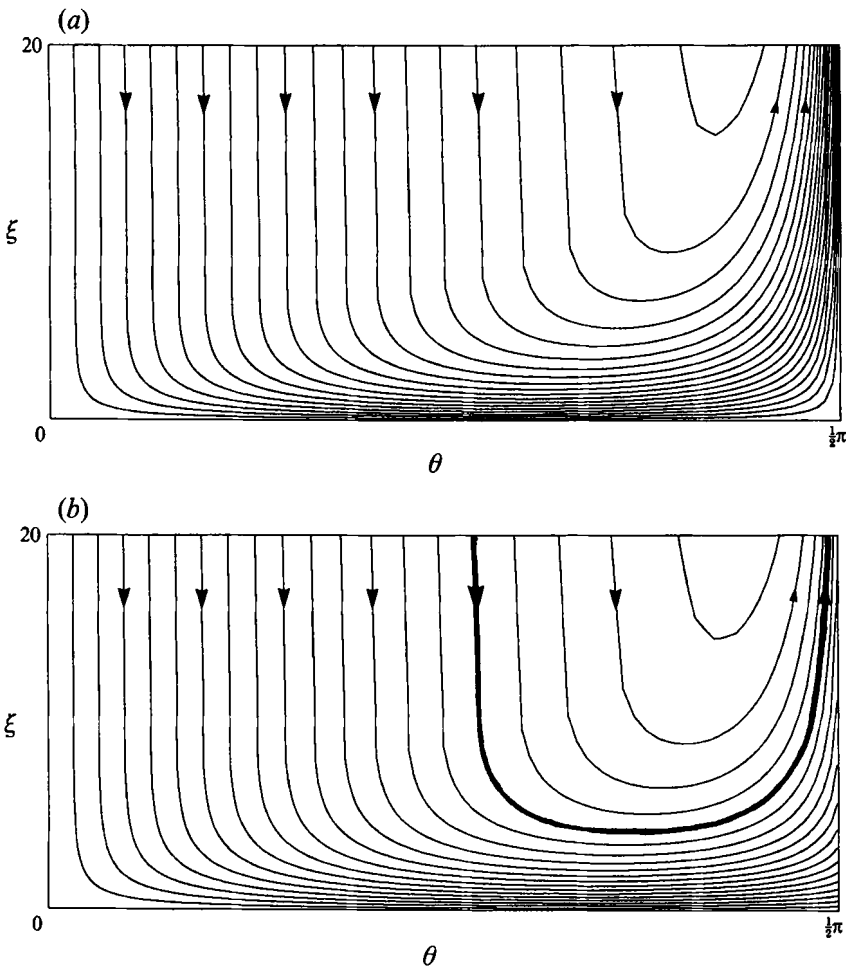$$-\bar{\lambda}(G')^2 + G' + G = 1, \qquad (3.23)$$

FIGURE 4. Streamlines for flow in the WBL. (a) $\bar{\lambda} = \frac{1}{4}$. The azimuthal velocity $\tilde{v}$ vanishes on each streamline, the end of the layer is locally stagnation-like and all fluid from the WBL spreads to pass through the shoulder region and enter the shear layer about $y = 1$. (b) $\bar{\lambda} = 1$. The azimuthal velocity vanishes at the layer end on streamlines with $\psi \geqslant \psi_s = 0.75$ and the outer flow is stagnation-like with one quarter of the WBL fluid spreading to pass through the shoulder region and enter the linear shear layer. Fluid on streamlines with $\psi < \psi_s$ continues onward through the shoulder region as a thin jet. The separating streamline $\psi = \psi_s$ is thickened.

with $G(0) = 0$ and $G(\infty) = 1$. This has the solution

$$G = 1 + (S^2 - 1)/4\bar{\lambda} \quad (0 < S < 1), \tag{3.24}$$

with S given implicitly by

$$S - (1 - 4\bar{\lambda})^{\frac{1}{2}} + \log \frac{1 - S}{1 - (1 - 4\bar{\lambda})^{\frac{1}{2}}} = -(\tfrac{1}{2}\pi - \theta)\,\xi \qquad (\bar{\lambda} \leqslant \tfrac{1}{4}). \tag{3.25}$$

In this solution $\tilde{v}$ vanishes on each streamline at the end of the WBL. Figure 4(a) gives streamlines for $\bar{\lambda} = \frac{1}{4}$ calculated by integrating (3.20) to give $\tilde{v}$ as a function of θ and then evaluating

$$\xi = \int_0^\psi \frac{\mathrm{d}\psi'}{\tilde{v}(\psi', \theta)} \tag{3.26}$$

to obtain the displacement of the streamline ψ. This pattern is typical of flows for $\bar{\lambda} \leqslant \frac{1}{4}$ with all entrained fluid expelled at the end of the layer through the stagnation flow.

Fluid from the WBLs passes through the shoulder regions to enter the shear layers about $y = \pm 1$ which are of the same form and carry the same mass as in linear flow. Except for the interior dynamics of the WBL the flow is unchanged from linear flow.

3.3.2. *The flow field for* $\bar{\lambda} = \lambda\alpha > \frac{1}{4}$ $\alpha \gg 1$

Once $\bar{\lambda} > \frac{1}{4}$ solution (3.25) is no longer valid. The WBL carries more fluid than can be expelled through the stagnation point into the shoulder region. Figure 4(b) gives streamlines of flow in the WBL for $\bar{\lambda} = 1$. For this value of $\bar{\lambda}$ the streamline $\psi_S = 0.75$, thickened in figure 4(b), divides the layer into two regions. On streamlines in the outer region where $\psi > \psi_S$ the tangential velocity vanishes as $\theta \to \frac{1}{2}\pi$ and a stagnation solution remains valid. On streamlines in the inner region where $\psi < \psi_S$ the tangential velocity is non-zero at $\theta = \frac{1}{2}\pi$ and no stagnation solution exists.

The general structure of the outer region for $\bar{\lambda} > \frac{1}{4}$ can again be found by looking for a solution of form (3.22) satisfying (3.23) with however the boundary condition $G(0) = \psi_S$, where as above ψ_S is the non-zero value of the streamfunction along the separating streamline at the edge of the continuing jet. A solution of form (3.24) exists with S given by

$$S + \log(1 - S) = -(\tfrac{1}{2}\pi - \theta)\xi + c, \tag{3.27}$$

provided G is restricted to the range $\psi_S \leqslant G \leqslant 1$, where

$$\psi_S = 1 - 1/4\bar{\lambda}, \tag{3.28}$$

and the constant of integration has been evaluated by requiring the streamline $G = \psi_S$ to follow the curve $(\tfrac{1}{2}\pi - \theta)\xi = c$. Since $c = G^{-1}(\psi_S) \to G^{-1}(0) = 0$ as $\bar{\lambda} \to \frac{1}{4}$ this solution merges with the solution in §3.3.1 as required. Equation (3.23) determines the velocity along ψ_S near $\theta = \frac{1}{2}\pi$ as $\tilde{v} = -\psi_\xi = -(\tfrac{1}{2}\pi - \theta) G' = -(\tfrac{1}{2}\pi - \theta)/2\bar{\lambda}$, which vanishes as $\theta \to \frac{1}{2}\pi$ as expected.

The tangential velocity on inner streamlines where $\psi < \psi_S$ remains non-zero as $\theta \to \frac{1}{2}\pi$ (satisfying the alternative condition that $1 + \bar{\lambda}\tilde{v}_\theta$ vanishes at the end of the layer) and so a fraction ψ_S of the fluid entrained into the WBL continues onwards. Only fluid following the outer streamlines enters the shoulder region and spreads to form the start of the shear layer about $y = 1$; the rest stays within a layer of thickness of order α^{-1} against the cylinder. This layer is governed once again by (3.15) and forms a detraining jet bound to the rear of the cylinder. The initial velocity profile $v(\psi)$ of the jet at $\theta = \frac{1}{2}\pi$ is given by the exit velocity profile of the continuing fluid from the WBL and must be determined numerically in general. The function $\tilde{v}(\psi)$ is positive for $\psi < \psi_S$ and vanishes for $\psi > \psi_S$, however the displacement ξ of the separating streamline ψ_S increases without limit as $\theta \to \frac{1}{2}\pi$ and so $\tilde{v}(\xi) > 0$ for all $\xi > 0$ at the start of the jet.

Information can propagate westwards from the jet and so, unlike the WBL, the far-field flow is not known completely *a priori*. The boundary conditions on the layer are thus

$$\psi(0, \theta) = 0, \quad \tilde{v}(\infty, \theta) = 0 \quad (\tfrac{1}{2}\pi < \theta < \pi). \tag{3.29}$$

As usual for a jet the precise form of the exterior flow, and thus the function $\psi_\infty(\theta)$, are determined by the solution of the boundary-layer equation, in this case (3.20). Numerical solutions are obtained for this equation by transforming the independent variables from (θ, ψ) to (θ, ϕ) where $\phi = \psi/\psi_\infty(\theta)$, so that the domain of ϕ is fixed at $0 \leqslant \phi \leqslant 1$, even within the range $\theta > \frac{1}{2}\pi$ where $\psi_\infty(\theta)$ is undetermined. Equation (3.20)
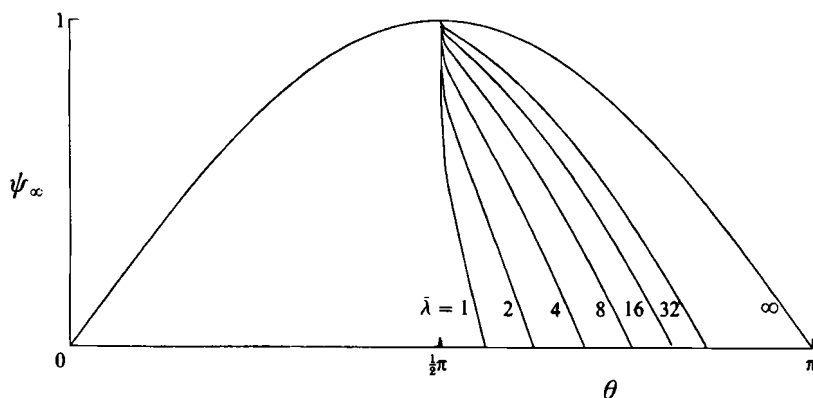
FIGURE 5. The streamfunction values at the outer edge of the detraining eastern boundary jet as a function of the azimuthal angle θ from the stagnation point at $\theta = 0$ through the shoulder region at $\theta = \frac{1}{2}\pi$ to the rear stagnation point at $\theta = \pi$. No fluid continues for $\bar{\lambda} = \frac{1}{4}$ and so $\psi_\infty(\theta) = 0$ for $\theta \geqslant \frac{1}{2}\pi$. With increasing $\bar{\lambda}$ more fluid enters the jet which however for finite $\bar{\lambda}$ always terminates before $\theta = \pi$. For $\bar{\lambda} \gg 1$ the jet starts with unit flux and continues to $\theta = \pi$ with $\psi_\infty(\theta) = \sin\theta$ for all $0 \leqslant \theta \leqslant \pi$.
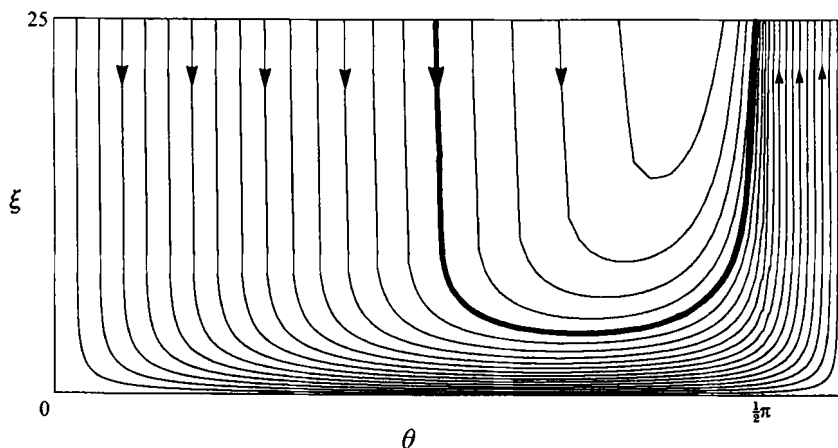

FIGURE 6. Streamlines of the complete structure for the layers of thickness α^{-1} when $\bar{\lambda} = 1$. One quarter of the fluid entering the WBL leaves through a singular stagnation point flow at the shoulder region and the remaining three-quarters detrains from a finite-length eastern boundary jet.

transforms from an ordinary differential equation into a hyperbolic partial differential equation subject to inflow boundary conditions at $\phi = 1$ for $0 \leqslant \theta < \frac{1}{2}\pi$. This system was solved using second-order finite differences, based on the box method, with the value of ψ_∞ determined iteratively in $\theta > \frac{1}{2}\pi$ using Newton's method to ensure that $\tilde{v} = 0$ at $\phi = 1$. The values of $\tilde{v}$ on $\phi = 0$ for $\theta > \frac{1}{2}\pi$, which form a boundary condition on the transformed equation, were obtained by integrating along $\phi = 0$ from $\theta = \frac{1}{2}\pi$. Figure 5 gives $\psi_\infty(\theta)$ from these calculations for various $\bar{\lambda} > \frac{1}{4}$, showing the jet terminating before $\theta = \pi$ at a point which moves further round the cylinder as $\bar{\lambda}$ increases. Figure 6 gives the flow pattern for the combined WBL and eastern jet at $\bar{\lambda} = 1$ showing the expected singularity at $\theta = \frac{1}{2}\pi$ for large values of ξ. One advantage of using the Von-Mises form (3.20) is that this singularity is resolved more easily.

Once $\psi_\infty(\theta)$ is determined the structure of the shear layers about $y = \pm 1$ and their merging at large $-x$ is fixed. In particular, for $X = \alpha^{-1}x$ and y both of order unity the
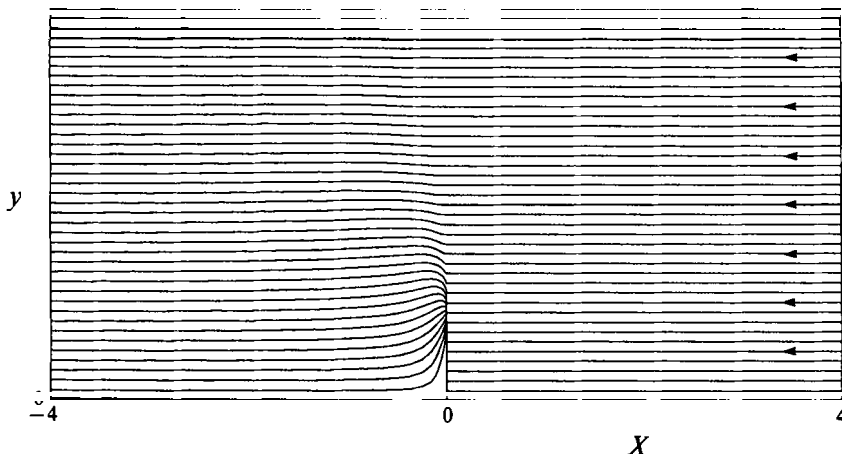
FIGURE 7. The streamline pattern for $X = \alpha^{-1}x$ of order unity and $\bar{\lambda} = 8$. Fluid passing through the shoulder region forms a point source of strength $\frac{1}{32}$ at $(0, 1)$ and fluid detraining from the eastern boundary jet gives a distributed source of total strength $\frac{31}{32}$ along $(0^-, y), 0 < y < 1$. The streamline interval is 0.1.
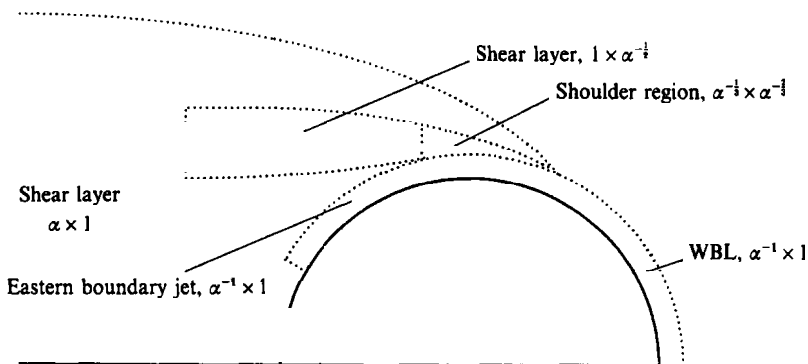

FIGURE 8. The postulated structure for attached flow when $\bar{\lambda} > \frac{1}{4}$. A fraction $1/4\bar{\lambda}$ of the fluid entrained into the WBL spreads in the shoulder region to enter the linear shear layer. The remaining fraction $1 - 1/4\bar{\lambda}$ of the WBL fluid continues along the cylinder as a finite-length detraining eastern boundary jet. The flow immediately outside the jet on the scale of the cylinder is no longer stagnant, being determined by (3.30).

merging layers are given by the solution of (3.6) that is odd in y and satisfies the initial condition

$$\psi(0, y) = \begin{cases} y, & y < 1 \\ \psi_\infty(\sin^{-1} y), & 0 \leqslant y < 1. \end{cases} \tag{3.30}$$

Here $\psi_\infty(\frac{1}{2}\pi) = \psi_S = 1 - 1/4\bar{\lambda}$ so the discontinuity in $\psi(0, y)$ at $y = 1$ represents a source of strength $1/4\bar{\lambda}$. The solution can be written

$$\psi = y + \frac{2}{\pi} \int_0^\infty \Psi(l) \exp{(l^2 X)} \sin{ly}\, dl, \tag{3.31}$$

$$\Psi(l) = \int_0^1 [\psi_\infty(\sin^{-1} y) - y] \sin{ly}\, dy. \tag{3.32}$$

For $\bar{\lambda} = \frac{1}{4}$ no fluid enters the eastern boundary jet, $\psi_\infty = 0$, the source at $(0, 1)$ has unit
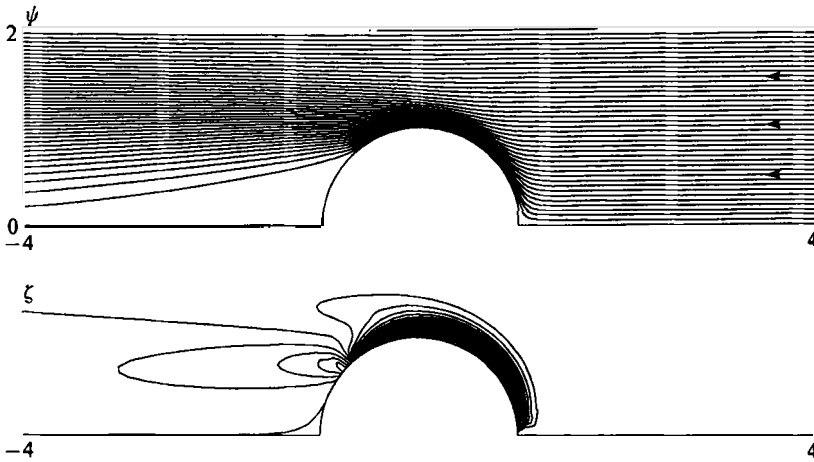
FIGURE 9. The streamlines and vorticity distribution from numerical integrations of the full equations for $\alpha = 32$ and $\lambda = \frac{1}{8}$ so $\bar{\lambda} = 4$. The vorticity pattern shows high-vorticity boundary fluid continuing round the cylinder region past the shoulder region at $\theta = \frac{1}{2}\pi$ and the streamlines show fluid detraining from the short eastern boundary jet which terminates at $\theta \approx 0.7\pi$ (cf. figure 5). The vorticity interval is 2.

strength and the flow is precisely the linear flow of two merging layers. As $\bar{\lambda}$ increases less fluid passes through the sources at $(0, \pm 1)$ and more into the eastern jet. Figure 7 gives streamlines calculated from (3.31) for $\bar{\lambda} = 8$. Fluid passing through the shoulder region forms a point source of strength $\frac{1}{32}$ at $(0, 1)$ and fluid detraining from the eastern boundary jet gives a distributed source of total strength $\frac{31}{32}$ over part of the rear of the obstacle. Figure 8 summarizes the structure presented here for attached flow when $\bar{\lambda} > \frac{1}{4}$ and figure 9 gives the streamline pattern and vorticity distribution from numerical integrations of the full equations for $\alpha = 32$ and $\lambda = \frac{1}{8}$ (so $\bar{\lambda} = 4$). The vorticity pattern shows the high-vorticity boundary fluid continuing round the cylinder past the shoulder region at $\theta = \frac{1}{2}\pi$ and the streamlines show fluid detraining from the short eastern boundary jet which terminates at $\theta \approx 0.7\pi$ (cf. figure 5). For $\bar{\lambda} \gg 1$ no fluid passes through the source and all fluid enters the jet, which then extends to $\theta = \pi$. The solution then takes the particularly simple form given in the following subsection.

3.4. The flow field for $\lambda \sim 1$, $\alpha \gg 1$

For faster flows where λ is of order unity (3.12), (3.13) show that the boundary layer at the front stagnation point thickens to have width $\delta = (\lambda/\alpha)^{\frac{1}{3}} = b$ for $\alpha \gg 1$. The WBL and eastern boundary jet thus also have thickness b and satisfy the inviscid form of (3.15),

$$\bar{u}\zeta_\xi + \bar{v}\zeta_\theta + \bar{v}\cos\theta = 0, \qquad (3.33)$$

where $\bar{u}$ and $\bar{v}$ are again polar velocity components defined as in (3.16) but with $\xi = (r-1)/b$ here. This scaling matches with that of §3.3 when $\lambda \sim \alpha^{-1}$. Equation (3.33) expresses the conservation of potential vorticity in the layer. The absence of viscous terms allows the far-field condition (3.17) to be applied to both layers, specifying the complete exterior flow for $0 \leqslant \theta \leqslant \pi$. Integrating across the layer gives

$$\overline{uv}_\xi + \overline{vv}_\theta + \psi\cos\theta = \tfrac{1}{2}\sin 2\theta \quad (0 \leqslant \theta \leqslant \pi), \qquad (3.34)$$

which has the solution $\psi(\xi, \theta) = H(\xi)\sin\theta$ provided H satisfies the ordinary differential equation

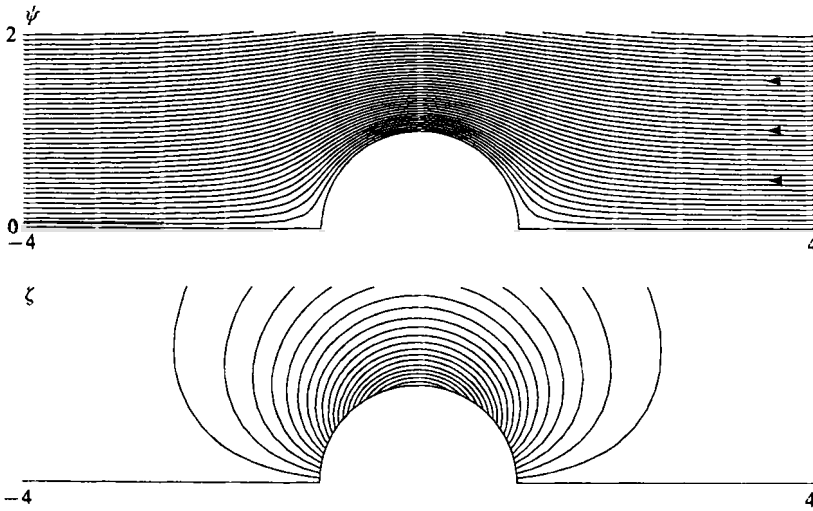$$-HH'' + H'H' + H = 1, \qquad (3.35)$$

FIGURE 10. The streamlines and vorticity distribution for the 'Long's model' solution (3.39) with $b = 1$. The vorticity interval is 0.05.

precisely the boundary-layer form of (3.9) in a layer of thickness $\alpha^{-\frac{1}{2}}$. The solution for the whole layer is thus

$$\psi(r, \theta) = \{1 - \exp[-(r-1)/b]\} \sin \theta. \tag{3.36}$$

All the oncoming flux with $0 \leqslant y \leqslant 1$ enters the WBL and is carried round the cylinder to be expelled through the eastern boundary jet. Outside these layers the flow is completely uniform.

3.5. *The flow field for $\lambda \gg 1$, $\alpha \gg 1$*

For large λ and α the flow on scales of order the cylinder diameter is governed by the conservation of potential vorticity. Equation (2.3) becomes

$$\frac{\partial(\psi, \zeta + b^{-2}y)}{\partial(x, y)} = 0, \tag{3.37}$$

where the Rossby wavelength scale b is now of order unity. For uniform upstream flow, integrating (3.37) along streamlines from $x \gg 1$ (where $\psi \to y$) gives the linear 'Long's model' problem

$$\nabla^2 \psi - b^{-2} \psi = -b^{-2}y. \tag{3.38}$$

Solutions of (3.38) consist of a uniform stream plus a contribution near obstacles decaying exponentially with scale b. Thus, for all b the flow on the viscous lengthscale α^{-1} is uniform and Ekman pumping is negligible everywhere. For λ of order unity b is small and the flow consists of an entraining WBL and detraining eastern jet, both of thickness b, as in the previous subsection. For large b the boundary flow weakens, the flow turns on scales of order the obstacle diameter and as $b \to \infty$ approaches irrotational flow. The streamfunction for flow past a circular cylinder, satisfying (3.38) and the impermeability condition $\psi = 0$ on $r = 1$ is

$$\psi = [r - K_1(br)/K_1(b)] \sin \theta, \tag{3.39}$$

similarly to Long (1952). Figure 10 gives streamlines from (3.39) for $b = 1$. These are indistinguishable from streamlines (not shown here) for $\lambda = \alpha = 32$ obtained by integrating the full nonlinear equations.
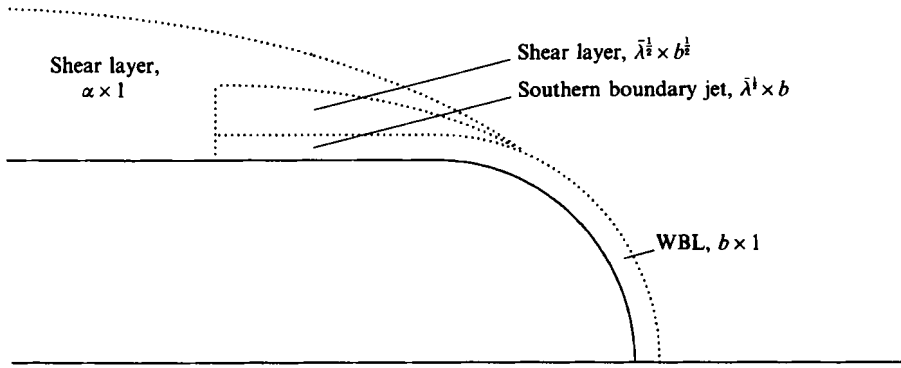
FIGURE 11. A schematic diagram of the asymptotic structure for westward flow past a 'cigar tube' obstacle. The structure for all values of $\bar{\lambda} = \alpha\lambda$ greater than $\frac{1}{4}$ up to $\bar{\lambda}$ of order α^2 is summarized in terms of $\bar{\lambda}$ and $b = (\lambda/\alpha)^{\frac{1}{3}}$. For $\bar{\lambda} \sim 1$ a detraining jet of length of order unity runs along $y = 1$. For $\bar{\lambda} \gg 1$ the jet thickens and lengthens. Over distances of order unity it conserves potential vorticity as in Long's model. Once $\bar{\lambda}$ is of order α^2 the southern boundary jet and the two linear shear layers merge to form a single nonlinear jet of thickness of order the obstacle width and length of order $\alpha \gg 1$.

3.6. *Longer obstacles*

The analysis above centres on obstacles of aspect ratio of order unity in general and for a circular cylinder in particular. Flow patterns for more elongated obstacles differ in some of the parameter regimes. Consider first westward flow past the 'cigar tube' with boundary

$$y = \begin{cases} 0, & 1 \leqslant x \\ \pm(1-x^2), & 0 \leqslant x \leqslant 1 \\ \pm 1, & x \leqslant 0. \end{cases} \tag{3.40}$$

Linear flow and nonlinear flow with $\bar{\lambda} \leqslant \frac{1}{4}$ are unchanged save solely that the shear layers at $y = \pm 1$ spread only outwards into $|y| > 1$. The dynamics change for $\bar{\lambda} > \frac{1}{4}$. The continuing fluid from the WBL can no longer form a detraining eastern jet and instead forms (in $y > 0$) a southern boundary jet along $y = 1, x < 0$, so called here as the jet runs along a southern boundary. The dynamics of this jet are discussed below and apply to any jet running precisely (for $\alpha \gg 1$) east–west or west–east and thus to jets along northern boundaries also. The flow structure in the three distinguished limits of increasing flow speed $\bar{\lambda} > \frac{1}{4}$, $\lambda \sim 1$ and $\lambda \sim \alpha$ can be compressed to the single structure illustrated in figure 11 by noting that the WBL has thickness of order b in each of these limits. Fluid from the WBL thus forms a jet of width b carrying flux of order unity. The scalings within the jet are equivalent to those introduced for mass-carrying layers in §3.4 with $\bar{y} = (y-1)/b$, $\bar{u} = -\psi_{\bar{y}} = bu$, and additionally $\bar{x} = x/\bar{\lambda}^{\frac{1}{2}}$. Integrating (2.3) across the layer gives

$$\bar{u}\bar{u}_{\bar{x}} + \bar{v}\bar{u}_{\bar{y}} = -\bar{u}, \tag{3.41}$$

where the constant of integration is evaluated by noting that since u is of order unity outside the layer, $\bar{u}$ vanishes to leading order as $\bar{y} \to \infty$. This is the equation for 'bottom frictional' jets discussed by Gadgil (1971) and for 'wide' jets by Page & Eabry (1990). It has the Von-Mises solution

$$\bar{u} = -\bar{x} + \bar{u}_0(\psi), \tag{3.42}$$

where $\bar{u}_0(\psi)$ is the velocity profile entering the jet from the end of the WBL. Equation (3.42) shows that $\bar{u}$ decreases linearly with $\bar{x}$ along each streamline so the jet terminates after a finite distance at the position $\bar{x}_s = \bar{u}_0(0)$ (where both of these quantities are
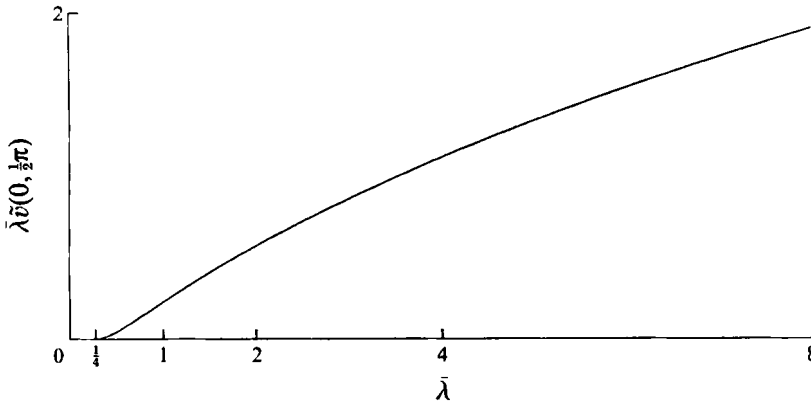
FIGURE 12. The length (in cylinder radii) of both the southern boundary jet along an extended obstacle of §3.6 and the separated jet in viscous flow past a bluff body of §5.1. The jets are absent for $\bar{\lambda} \leqslant \frac{1}{4}$ and their length approaches $\bar{\lambda}^{\frac{1}{2}}$ for $\bar{\lambda} \gg 1$. This structure applies when $\alpha \gg 1$ and $\lambda \ll \alpha$, i.e. $\bar{\lambda} \ll \alpha^2$.

negative). Figure 12 shows the variation with $\bar{\lambda}$ of the length of the jet in units of cylinder radii, i.e. $-\bar{\lambda}^{\frac{1}{2}}\bar{u}_0(0) = \bar{\lambda}\bar{v}(0,\frac{1}{2}\pi)$, where $\bar{v}$ follows straightforwardly by integrating (3.20) along $\psi = 0$ from $\theta = 0$ to $\frac{1}{2}\pi$. The jet is absent for $\bar{\lambda} \leqslant \frac{1}{4}$ and, as expected from the discussion of the southern boundary jet in II, increases smoothly with $\bar{\lambda}$ for $\bar{\lambda} > \frac{1}{4}$. The large-$\bar{\lambda}$ behaviour follows from noting from (3.36) that $\bar{v} \to b^{-1}$ as $\bar{\lambda} \to \infty$ so the jet length approaches $\bar{\lambda}^{\frac{1}{2}}$. The first stages of this asymptotic behaviour are apparent in figure 12.

This nonlinear jet of width $y-1 \sim b$ and length $-x \sim \bar{\lambda}^{\frac{1}{2}}$ lies within the linear shear layer. The value $\psi_\infty(\bar{x})$ of ψ at the outer edge of the jet (where $\bar{u} = 0$) is given implicitly by the solution of

$$\bar{u}_0(\psi_\infty) = \bar{x},\qquad(3.43)$$

and (3.43) then forms the boundary condition along $y = 1$ for the shear layer. This structure shows particularly clearly when $\bar{\lambda}$ is sufficiently large that the entire WBL flow enters the jet. Then (3.39) gives $\bar{u}_0(\psi) = \psi - 1$ so (3.42) gives $\psi = (1+\bar{x})(1-e^{-\bar{y}})$ and (3.43) gives $\psi_\infty = 1+\bar{x}$. The jet terminates when $\bar{x} = -1$. Jets for smaller $\bar{\lambda}$ terminate earlier.

The shear layer forced by the jet outflow has length of order $\bar{\lambda}^{\frac{1}{2}}$ and thus, from (3.1), width of order $b^{\frac{1}{2}}$. It is governed by (3.4) (with $\bar{x}$ replacing x and $\ddot{y} = (y-1)/b^{\frac{1}{2}}$ replacing $\hat{y}$) subject to the boundary conditions

$$\psi(0,\ddot{y}) = 1, \quad \psi(\bar{x},0) = \psi_\infty(\bar{x}),\qquad(3.44)$$

and a solution similar to (3.31), (3.32) follows directly. On the lengthscale of $X = x/\alpha$ the layer is unaltered from the corresponding shear layer in linear flow.

The structure of figure 11 holds for $\frac{1}{4} < \bar{\lambda} \ll \alpha^2$. For faster flows, where $\lambda \sim \alpha \gg 1$ (so $\bar{\lambda} \sim \alpha^2, b \sim 1$), the WBL has thickness of order unity, governed by the conservation of potential vorticity through Long's model, and the southern boundary jet and shear layers merge to form a nonlinear, detraining jet of thickness unity and length of order α governed by equation (5.1) of I. Solutions of this latter equation have a wider significance for flow over long obstacles and will be discussed elsewhere. The layer structure for obstacles with east–west boundary sections of finite, non-zero length follows directly by combining the 'cigar tube' structure discussed here with the detraining eastern jet of §§3.3–3.5.

4. Eastward flow

Eastward flow is governed by (2.3)–(2.6) with the negative sign chosen in (2.6). For slow steady flow where α is arbitrary and $\lambda \ll \min(\alpha^{-1}, 1)$, the vorticity equation (2.3) reduces to (3.1) as in westward flow. The solution with uniform eastward flow at large distance is thus given by multiplying solution (3.2) by -1. The pattern of streamlines is unaltered. Oncoming flow displaced into shear layers about $y = \pm 1$ passes through shoulder regions at $(x, y) = (0, \pm 1)$ and enters a detraining WBL on the rear of the cylinder.

4.1. *The flow near the rear stagnation point*

The stagnation point at $(x, y) = (1, 0)$, which for westward flow is an entraining forward stagnation point in a WBL, is in eastward flow a detraining rear stagnation point. The full governing equation (2.3) again has a solution of similarity form (3.8) where F here satisfies (3.9) with α replaced by $-\alpha$ on the right-hand side. This has the exact solution $F(x) = -1 + \exp(-x/\delta)$, satisfying the far-field condition $F(\infty) = -1$, provided $\alpha\delta^2 - \delta + \lambda = 0$. The two roots for δ are

$$\delta_1 = [1 + (1 - 4\alpha\lambda)^{\frac{1}{2}}]/2\alpha, \quad \delta_2 = [1 - (1 - \alpha\lambda)^{\frac{1}{2}}]/2\alpha, \tag{4.1}$$

which, as required, are both positive and real for $\bar{\lambda} = \alpha\lambda < \frac{1}{4}$. For weak advection $(\lambda \to 0)$, $\delta_1 \to \alpha^{-2}$ and $\delta_2 \to 0$. The layer that evolves smoothly with increasing flow speed from the linear layer is thus the layer of thickness δ_1.† As $\bar{\lambda}$ increases, this layer thins and the simple stagnation-point solution vanishes as $\bar{\lambda}$ passes through $\frac{1}{4}$ and the roots (4.1) become complex. The roots continue to give the oscillatory behaviour of the outer part of the boundary layer and it is the presence of two roots that allows the unusual boundary condition at the exterior of the nonlinear WBL in §4.2. Although the layer is detraining, which usually precludes specifying precisely the outer flow field (as in the eastern jet of §3.3.2), the presence of two decaying solutions of unspecified amplitude allows the exterior streamfunction itself to be specified as for an entraining boundary layer (like the WBL of §3.3).

Since both roots (4.1) have positive real part, the similarity form does not yield a stagnation-point solution for the flow at the forward stagnation point $(x, y) = (-1, 0)$. In contrast to the detraining eastward jet in westward flow, the absence here of any decaying solutions for the outer regions of the boundary layer precludes an entraining eastern boundary layer irrespective of the strength of the oncoming flow.

4.2. *The flow field for $\lambda \sim \alpha^{-1}$, $\alpha \ll 1$*

As noted in §3.3 and I nonlinearity first becomes important in the WBL for $\bar{\lambda}$ of order unity. The shear layers remain linear and the shoulder regions turn the oncoming flow to form the start of the WBL. The layer is again of thickness α^{-1} and analogously to §3.3 is governed by

$$\bar{\lambda}\tilde{v}\tilde{v}_\theta + \tilde{v} + \psi\cos\theta = -\tfrac{1}{2}\sin 2\theta, \tag{4.2}$$

$$\psi(0, \theta) = 0, \quad \psi(\infty, \theta) = -\sin\theta \quad (0 < \theta < \tfrac{1}{2}\pi). \tag{4.3}$$

The solution of (4.3) for $\bar{\lambda} \leqslant \frac{1}{4}$ is discussed in Foster (1985) and I and follows directly by integrating (4.3) along streamlines to obtain $\tilde{v}(\psi, \theta)$ and then evaluating (3.26) to obtain the displacement of streamlines. Provided $\bar{\lambda} \leqslant \frac{1}{4}$ all fluid entering the WBL from the shoulder region detrains by the rear stagnation point at $\theta = 0$.

For $\bar{\lambda} > \frac{1}{4}$ this is no longer the case and the azimuthal velocity $-\tilde{v}$ remains positive

† This root is given in II. However δ in II equals δ_1^{-1} here and (14) in II should have δ replaced by δ^{-1}.
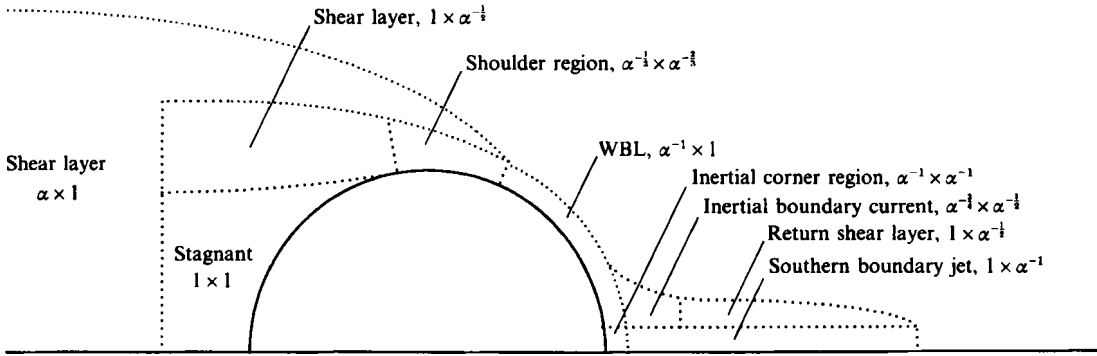
FIGURE 13. A schematic diagram of the asymptotic structure of eastward flow past a cylinder when $\bar{\lambda} = \alpha\lambda$ is of order unity but greater than $\frac{1}{4}$.

as $\theta \to 0$ on those streamlines closest to the cylinder. Simple stagnation flow at $\theta = 0$ breaks down. The flow at a rear stagnation point when $\bar{\lambda} > \frac{1}{4}$ is examined in detail for a model problem in II where an asymptotic structure is presented supported by accurate numerical computations. Figure 13 gives a schematic diagram of this structure, modified for the present geometry. The continuing flow from the WBL is turned in a square inertial region of dimension $\alpha^{-1} \times \alpha^{-1}$ where the governing equation is the conservation of relative vorticity. The incoming southward velocity profile is simply turned to give the outgoing eastward velocity profile for a detraining southern boundary jet of dimensions $1 \times \alpha^{-1}$ along $y = 0$. The eastward jet, governed by equations equivalent to (3.41) and (3.42), has length of order $\bar{\lambda}$ and forms the southern boundary condition for a shear layer of dimensions $1 \times \alpha^{-\frac{1}{2}}$ governed by (3.4) that returns fluid to the west. This returning fluid rejoins the WBL in an inertial boundary current of dimensions $\alpha^{-\frac{3}{4}} \times \alpha^{-\frac{1}{4}}$ governed by the conservation of potential vorticity.

Unlike the asymptotic structure for westward flows in §§3.4 and 3.5, the structure for eastward flows does not remain locally determined if the speed increases so that λ becomes of order unity or larger. This appears to be closely related to the upstream influence problem discussed in I. Similarly, no new structure appears for elongated obstacles like those in §3.6. For obstacles like (3.40) corresponding to eastward flow over an abrupt southward step the sole difference from flow past a cylinder is that the upstream linear shear layers spread into only $|y| > 1$. Flow over a northward step is even simpler: the flow is displaced northwards over distances x of order α without forming flux-carrying shear layers, and remains linear for speeds up to those where $\lambda \sim \alpha \gg 1$.

5. Viscous separation

This paper considers the limit of Ekman and Rossby numbers vanishing with $\lambda = Ro/2E^{\frac{1}{2}}$ fixed. In this limit Ekman pumping by Ekman layers on the upper and lower boundaries gives the leading-order viscous effect on an otherwise inviscid motion. Horizontal viscous effects are negligible in the bulk of the flow, becoming important only within thin boundary layers on the vertical sides of obstacles. Provided these layers remain thin and attached to the obstacles they do not affect the flow. If the layers separate then the leading-order flow in the neighbourhood of the obstacle alters. A review of results on the separation of $E^{\frac{1}{3}}$ layers on an f-plane is given in Page (1987). In particular Page (1982) notes that attached flow can be expected on an f-plane provided

$$\lambda \frac{\mathrm{d}u_0}{\mathrm{d}s} \geqslant -1 \qquad (5.1)$$

at each point on the boundary. Here u_0 is the tangential velocity and s is the distance along the boundary in the flow direction. The discussion in Page (1987) and the numerical solutions for f-plane flows in Becker (1991) show further that the shape of the separated region can be obtained by choosing the region boundary so that equality holds in (5.1) at each point on the boundary.

The linear solutions ($\lambda = 0$) of §3.1 and nonlinear solutions of §3.3 for $\bar{\lambda} \leqslant \frac{1}{4}$ can be regarded as separated flows. An $E^{\frac{1}{4}}$ layer forms on the incident side of the cylinder with the fluid accelerating before separating at the shoulder regions at $\theta = \pm\frac{1}{2}\pi$. No $E^{\frac{1}{4}}$ layer is required on the western side of the cylinder as the flow is stagnant there to leading order, and no $E^{\frac{1}{4}}$ layers are present within the linear shear layers as the leading-order flow is arbitrarily differentiable there. Once $\bar{\lambda} > \frac{1}{4}$ in the inviscid solution of §3.3.2 some fluid enters an eastern boundary jet along the rear of the cylinder. The flow decelerates within this jet and may separate. This is considered in the following subsection.

5.1. *A structure for westward separated flow*

While the $E^{\frac{1}{4}}$ layer remains attached to the cylinder it brings the non-zero slip velocity along $\psi = 0$ at the inner limit of the mass-carrying layer of §3.3 to rest at the cylinder surface. Suppose the flow is symmetric about $y = 0$ and the $E^{\frac{1}{4}}$ layer remains attached in $y > 0$ from the front stagnation point F until a point S where the layer separates tangentially from the cylinder. Denote the path of the separated streamline by SA and introduce normal and tangential coordinates rotated through an angle $\gamma(s)$ from Oxy, with arclength s measured from S (figure 14a). The $E^{\frac{1}{4}}$ layer matches a discontinuity in tangential velocity across SA and a mass-carrying of thickness b matches a discontinuity (on the scale of the cylinder radius) in ψ across SA. The equation governing the mass-carrying layer in these coordinates (with $\tilde{u} = u/\alpha$) follows similarly to (3.20) as

$$\bar{\lambda}\tilde{u}\tilde{u}_s + \tilde{u} - \psi \sin\gamma(s) = -\psi_\infty(s)\sin\gamma(s), \qquad (5.2)$$

along lines $\psi = $ constant. Here $\psi_\infty(s)$ is non-zero, specifying the detraining of fluid from the layer into the external flow in $n > 0$. Including the $E^{\frac{1}{4}}$ layer viscous terms in (5.2) and integrating across the $E^{\frac{1}{4}}$ layer at $\psi = 0$ then gives the $β$-plane extension (for $\alpha \gg 1$) of the free-streamline condition in Page (1987), i.e.

$$\lambda u_0 \frac{\mathrm{d}u_0}{\mathrm{d}s} + u_0 = -\alpha\psi_\infty(s)\sin\gamma(s) \qquad (5.3)$$

along the separated streamline.

Equation (5.3) can be expected to have two solutions for the tangential velocity $u_0(s)$: one, $u_0^-(s)$ say, corresponding to the flow just inside the separated streamline $\psi = 0$ and the other, $u_0^+(s)$ say, corresponding to flow just outside the streamline $\psi = 0$ and so forming the inner boundary condition of the separated mass-carrying layer. Now u_0^- vanishes at the separation point S and ψ_∞ is non-zero there for $\bar{\lambda} > \frac{1}{4}$. Equation (5.3) thus requires that γ vanishes there: the flow separates at $\theta = \frac{1}{2}\pi$ for all $\bar{\lambda} > \frac{1}{4}$. Now suppose that $\gamma(s)$ is positive at some $s > 0$. From (5.3) this would imply that u_0^- is negative there, giving within the separated region an order-unity flow counter to the free-stream flow. This flow pattern would differ from the numerical integrations for $β$-plane flows of Matsuura & Yamagata (1986) and the f-plane integrations of Becker
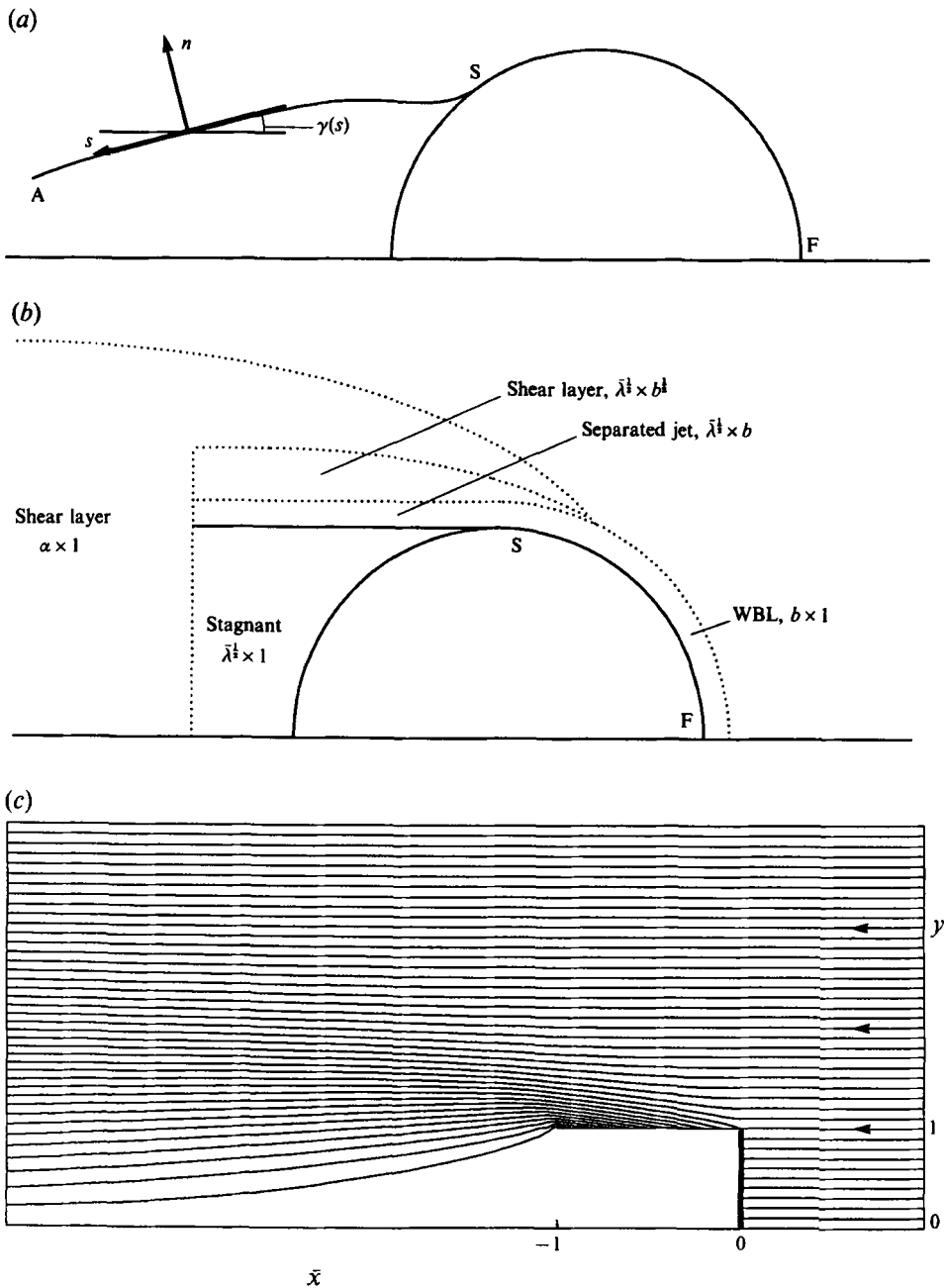
(a)

n

S

s

$\gamma(s)$

A

F

(b)

Shear layer, $\bar{\lambda}^{\frac{1}{2}} \times b^{\frac{1}{2}}$

Separated jet, $\bar{\lambda}^{\frac{1}{2}} \times b$

Shear layer
$\alpha \times 1$

Stagnant
$\bar{\lambda}^{\frac{1}{2}} \times 1$

S

WBL, $b \times 1$

F

(c)

y

1

0

-1 0

$\bar{x}$

FIGURE 14. A structure for separated westward flow when $1/4\alpha \leqslant \lambda \ll \alpha$. (a) The coordinate system. Flow enters a mass-carrying boundary layer at the front stagnation point F and separates tangentially at S. Tangential and normal coordinates s and n are rotated through an angle $\gamma(s)$ from Oxy, with arclength s measured from S. (b) The postulated structure in $y > 0$. Fluid from the WBL passes into a finite-length jet lying along $y = 1$. The jet detrains into $y > 1$ leaving the region immediately behind the cylinder stagnant. This detrained fluid spreads into $y < 1$ within a shear layer of length of order α of exactly the same tapering structure as the equivalent layer in the linear flows of figures 1 and 2. To leading order the length of the separated region is proportional to α. (c) Streamlines for large $\bar{\lambda}$ and $b = 0.1$ on the jet-length scale, $\bar{x} = x/\bar{\lambda}^{\frac{1}{2}}$, showing for y of order unity the basic flow and the shear layer forced by the detraining jet. The cylinder and WBL become the line $\bar{x} = 0$, $0 < y < 1$ and the jet the line $-1 < \bar{x} < 0$, $y = 1$.

(1991). It thus appears that $\gamma \equiv 0$ and $u_0^- \equiv 0$ along the entire length of the separated $E^{\frac{1}{4}}$ layer. As a result, the flow is stagnant close to the rear of the cylinder and the separated streamline $\psi = 0$ lies along $y = 1$.

With $\gamma = 0$ equation (5.2) is equivalent to (3.41) and the flow in the mass-carrying layer along $y = 1^+$ is determined exactly as in §3.6 for the layer along a longer obstacle. As there, the structure over the wide range from $\bar{\lambda} > \frac{1}{4}$ to $\lambda \ll \alpha$ can be condensed to a single form. The separated jet has thickness b, finite length $\lambda u_0(0)$ of order $\bar{\lambda}^{\frac{1}{2}}$ (shown as a function of $\bar{\lambda}$ in figure 12), and lies within a linear shear layer of length of order $\bar{\lambda}^{\frac{1}{2}}$ and width of order $b^{\frac{1}{2}}$. An example of this structure for large $\bar{\lambda}$ is given in figure 14(*c*) for $b = 0.1$. Here (3.4) has been integrated subject to (3.43) using the large-$\bar{\lambda}$ result of §3.6 that $\psi_\infty 1 = 1 + \bar{x}$.

On the scale of $X = x/\alpha$ the flow field is of precisely the same form as linear flow: there are sources of unit strength at $(0, \pm 1)$ from which fluid spreads to fill the stagnant region behind the cylinder (figure 14*b*). There is no separation bubble as such. Unusually, the separated flow on this scale more closely resembles linear flow than attached nonlinear flow (where fluid detrains from a distributed source on the rear of the cylinder as illustrated by figure 7). Provided λ is small compared to α the size of the stagnant region is independent of λ to leading order and the length of the streamline pattern scales on α. For λ of order α the various layers behind the cylinder merge into a single layer as in §3.6.

5.2. *Comparison with observed flows*

Experimental observations of separation behind circular cylinders in westward flows on a β-plane are reported by Boyer & Davies (1982, called BD herein). BD concentrate on determining the variation of the length of the separated region as a function of the various non-dimensional parameters describing the flow. They note a difficulty in ascribing a definite length to a separation bubble and instead present results for the distance behind the cylinder by which dye streaks released separately from the cylinder surfaces in $y > 0$ and $y < 0$ have converged to within one-fifth of a cylinder radius. The structure put forward in §5.1 and illustrated by figure 14(*c*) shows that even this definition is not necessarily robust. The length determined in this manner would depend on the value of the streamfunction along the streakline: for the streamline $\psi = \epsilon > 0$ the distance of approach to the axis $y = 0$ increases as $-\log \epsilon$ as $\epsilon \to 0$. This weak dependence on ϵ may not be significant in the experiments.

On the assumption that in different experiments the inner streakline corresponds to approximately the same streamfunction value, the eddy lengths observed by BD should increase linearly with α provided α is large and λ remains small compared to α. The parameter definitions in BD differ slightly from those here. In terms of the parameters in BD the present parameters become

$$\alpha = \hat{\beta} H \widehat{Ro} / R(2Ek)^{\frac{1}{2}}, \quad \lambda = H \widehat{Ro} / R(2Ek)^{\frac{1}{2}}, \tag{5.4}$$

where a hat has been added to symbols used both here and in BD to denote their form in BD. In summarizing their results BD note that when westward flow around a cylinder separates the length of the separated region:

    (i) increases with increasing $\widehat{Ro}$,
    (ii) increases with increasing $\hat{\beta}$,
    (iii) decreases with increasing R/H,
    (iv) decreases with increasing Ek.

This behaviour is consistent with a separation region proportional to α.

Two particularly clear plates with reasonably strong β-effect in BD are their figure

$5(c)$ and the westward flow with $\hat{\beta} = 1$ in their figure 26. Both plates show flows with the general form of the linear flows of figure 1 as expected. The corresponding values of (α, λ) are $(1.4, 1.8)$ and $(3.1, 3.1)$. These would predict that the separated region in figure 26 of BD should be twice as long as that in their figure $5(c)$. The streaklines in the two plates do not show this. As noted above the streaklines might follow different streamline values; some support for this comes from noting that the separation bubble in figure $26(a)$ appears to be of a similar size to that in figure $26(b)$ where $\alpha \approx 0.8$. It should also be noted that α is not large in figure $5(c)$ so Ekman pumping is as strong as vortex stretching there. The thicknesses $b = (\lambda/\alpha)^{\frac{1}{2}}$ for the mass-carrying layers in the two figures are 1.1 and 1.0. These are significantly thicker than the $E^{\frac{1}{4}}$ layers, of thicknesses $\hat{\delta} = dE^{\frac{1}{4}}/\sqrt{2}$ of about 0.2 and 0.1 respectively, and so the general theory of §5.1 can be expected to apply. However the mass-carrying layers are not thin compared to the cylinder radius and so the description of the wake region in terms of three distinct layers is not strictly applicable.

Among their numerical computations for viscous westward flows Matsuura & Yamagata (1986) specifically model some of BD's experiments. The streamline and vorticity patterns of their figure $2(c)$ with $(\alpha, \lambda, \hat{\delta}) = (1.41, 1.77, 0.161)$ to model BD's figure $5(c)$, show the flow separating at the shoulders of the cylinder and layers extending westwards, rather than approaching and joining as in the corresponding eastward flow. The slight deviation downwards from the line $y = 1$ is probably caused by the displacement effect in the asymmetric $E^{\frac{1}{4}}$ layer. The patterns in their figure 6, with $(\alpha, \lambda, \hat{\delta}) = (15, 10, 0.1)$, $(3, 2, 0.02)$ and $(1.5, 1, 0.01)$ in (a), (b), and (c) respectively, are also broadly consistent with the structure presented above, as is their figure 8 which shows the wake length increasing linearly with $\hat{\beta}$ at large Reynolds number. A further feature confirmed by Matsuura & Yamagata is the insensitivity to changes in the flow parameters of the position of the point of separation in westward flows: the flow always separates at the top of the obstacle.

The structure proposed here differs significantly from the flows postulated by Merkine (1980) who assumes that the unseparated solution of (3.39) always gives the flow external to the viscous $E^{\frac{1}{4}}$ boundary layer even when the $E^{\frac{1}{4}}$ layer solution he then calculates separates from the cylinder. His prediction that westward flow separates at $\theta = 1.78$ ($102°$) cannot be considered reliable.

5.3. Eastward separated flow

Separation in eastward flows is discussed in Foster (1985) and I but determining the structure of the separated region is less straightforward than in westward flows. Provided $\bar{\lambda} \leqslant \frac{1}{4}$ the $E_{\frac{1}{4}}$ layer within the WBL in eastward flow remains attached to the cylinder. Once $\bar{\lambda} > \frac{1}{4}$ condition (5.1) for attached flow is violated close to the rear stagnation point. The flow separates but arguments similar to those in §5.1 show that the separated streamline is no longer restricted to lines $y = \text{constant}$ but can slope steeply to confine the separated flow to a finite region in the neighbourhood of the rear stagnation point. The obstacles treated in I were chosen to be streamlined partly because inviscid calculations for such shapes could be expected to closely approximate viscous flows with attached boundary layers and separated viscous flows. The general structure of the flow outside the separated region remains that of figure 13 with excess mass from the WBL forming a southern boundary jet along the axis $y = 0$.

6. Summary

This paper has considered flow past bluff bodies in both eastward and westward flows in the almost-inviscid, infinite-Reynolds-number limit of $Ro \to 0$, $E \to 0$ with $\lambda = Ro/2E^{\frac{1}{2}}$ fixed. For westward flows a complete structure in the limit of vanishingly small Ekman pumping ($\alpha \gg 1$) has been obtained for all strengths of nonlinearity λ from linear flow ($\lambda = 0$) through to purely inviscid flow conserving potential vorticity everywhere ($\lambda \sim \alpha \gg 1$). For eastward flows a complete structure has been presented for the regime in which nonlinearity first becomes important ($\lambda \sim \alpha^{-1} \ll 1$).

One unusual and unexpected result of the analysis of eastward flow is the conclusion that a western boundary layer (WBL) in this parameter regime can match any interior flow. If the layer is entraining then the presence of a single decaying solution for the exterior of the layer shows that the vorticity and mass flux in the layer is determined by the exterior flow, i.e. by the entrained fluid. If the layer is detraining then the presence of two decaying solutions for the exterior of the layer allows the layer to match any specified exterior flow. Thus in this limit, as for linear flow, the WBL is passive, simply transferring mass to match the interior flow.

Horizontal viscous effects in these flows are confined to layers of thickness $E^{\frac{1}{4}}$ which are thinner than the mass-carrying western boundary layers and their extensions discussed elsewhere in this work provided $\tan \beta \ll E^{\frac{1}{4}}$. If the $E^{\frac{1}{4}}$ layers remain attached they do not affect the external flow. Once $\bar{\lambda} = \alpha\lambda$ exceeds some critical value in flows past bluff bodies these layers separate. The results in §3 then lead directly to the proposed structure for separated flow in §5. Unlike the wide and spreading separation bubbles of non-rotating, infinite-Reynolds-number flows (Smith 1985, 1986 and Fornberg 1985), the separated regions predicted here and observed in experiments are no wider than the obstacle producing them.

The present structures demonstrate why Long's (1952) theory for westward flows differs from both his and Boyer & Davies' (1982) experiments and from Matsuura & Yamagata's (1986) integrations. Long's model is at the advection-dominated end of the continuous spectrum of almost-inviscid flow development which stretches, with increasing flow speed, from the linear flows of figures 1 and 2 through the flows with attached detraining eastern boundary jets of figures 8 and 9 to the potential-vorticity-conserving flows of figure 10. Since the numerical method used here retains time-dependence and allows wave propagation both upstream and downstream, this smooth continuum of flows belies Matsuura & Yamagata's comment that it is westward long-wave propagation that accounts for the difference between Long's model and experimental observations. The experiments and viscous numerical flows bifurcate smoothly from the almost-inviscid continuum when $\bar{\lambda}$ exceeds some critical value of order unity ($\frac{1}{4}$ for the circular cylinder) and the $E^{\frac{1}{4}}$ layer separates at the shoulders of the obstacle to form detached jets, of the same thickness as the WBL, within the linear shear layers along lines $y = $ constant. It is viscous separation that accounts for the differences.

In their experimental observations of flow in a spherical shell Fultz & Long (1951) note that there are velocity discontinuities or vortex sheets on either side of the wake behind a cylinder in westward flow whereas there is only one such surface behind a cylinder in eastward flow; comparing the patterns for eastward and westward flows with $\hat{\beta} = 0.25$ in figure 26 of BD shows the differences clearly. The structures proposed here for these flows and illustrated in figures 13 and 14(*b*) have these properties with a single jet along $y = 0$ in eastward flow and twin jets along $y = \pm 1$ in westward flow.

REFERENCES

BECKER, A. 1991 The separated flow past a cylinder in a rotating frame. *J. Fluid Mech.* **224**, 117–132.

BOYER, D. L. & DAVIES, P. A. 1982 Flow past a circular cylinder on a β-plane. *Phil. Trans. R. Soc. Lond.* A **306**, 533–556 (referred to herein as BD).

FORNBERG, B. 1985 Steady viscous flow past a circular cylinder up to Reynolds number 600. *J. Comput. Phys.* **61**, 297–320.

FOSTER, M. R. 1985 Delayed separation in eastward rotating flow on a β-plane. *J. Fluid Mech.* **155**, 59–75.

FULZ, D. & LONG, R. R. 1951 Two-dimensional flow around a circular barrier in a rotating spherical shell. *Tellus* **3**, 61–68.

GADGIL, S. 1971 Structure of jets in rotating systems. *J. Fluid Mech.* **47**, 417–436.

HIDE, R. & HOCKING, L. M. 1979 On detached shear layers and western boundary currents in a rotating homogeneous liquid. *Geophys. Astrophys. Fluid Dyn.* **14**, 19–43.

LONG, R. R. 1952 The flow of a liquid past a barrier in a rotating spherical shell. *J. Met.* **9**, 187–199.

MATSUURA, T. & YAMAGATA, T. 1986 A numerical study of a viscous flow past a right circular cylinder on a β-plane. *Geophys. Astrophys. Fluid Dyn.* **37**, 129–164.

MERKINE, L.-O. 1980 Flow separation on a β-plane. *J. Fluid Mech.* **99**, 399–409.

PAGE, M. A. 1982 Flow separation in a rotating annulus with bottom topography. *J. Fluid Mech.* **123**, 303–313.

PAGE, M. A. 1987 Separation and free-streamline flows in a rotating fluid at low Rossby number. *J. Fluid Mech.* **179**, 155–177.

PAGE, M. A. & EABRY, M. D. 1990 The breakdown of jets flows in a low-Rossby-number rotating fluid. *J. Engng Maths* **24**, 287–310.

PAGE, M. A. & JOHNSON, E. R. 1990 Flow past cylindrical obstacles on a β-plane. *J. Fluid Mech.* **221**, 349–382 (referred to herein as I).

PAGE, M. A. & JOHNSON, E. R. 1991 Nonlinear western boundary current flow near a corner. *Dyn. Atmos. Oceans* **15**, 477–504 (referred to herein as II).

SMITH, F. T. 1985 A structure for laminar flow past a bluff body at high Reynolds number. *J. Fluid Mech.* **155**, 175–191.

SMITH, F. T. 1986 Concerning inviscid solutions for large-scale separated flows. *J. Engng Maths* **20**, 271–292.

WAECHTER, R. T. 1968 Steady longitudinal motion of an insulating cylinder in a conducting fluid. *Proc. Camb. Phil. Soc.* **64**, 1165–1201.

WAECHTER, R. T. & PHILLIPS, J. R. 1985 Steady two- and three-dimensional flows in unsaturated soil: the scattering analogue. *Water Resources Res.* **21**, 1875–1887.